Supplementary Information for

Multi-quantum well nanowire heterostructures for wavelength-controlled lasers

Fang Qian[1], Yat Li[1]*, Silvija Gradečak[1†], Hong-Gyu Park[1‡], Yajie Dong[1], Yong Ding[2], Zhong Lin Wang[2¶] and Charles M. Lieber[1,3¶]

[1]Department of Chemistry and Chemical Biology, Harvard University, Cambridge, Massachusetts 02138, USA

[2]School of Materials Science and Engineering, Georgia Institute of Technology, Atlanta, GA 30332, USA

[3]School of Engineering and Applied Sciences, Harvard University, Cambridge, Massachusetts 02138, USA

*Present address: Department of Chemistry and Biochemistry, University of California, Santa Cruz, California 95064, USA

[†]Present address: Materials Science & Engineering, Massachusetts Institute of Technology, Cambridge, Massachusetts 02139, USA

[‡]Present address: Department of Physics, Korea University, Seoul 136-713, Korea

[¶]email: zhong.wang@mse.gatech.edu; cml@cmliris.harvard.edu

Index

Supplementary Methods
Supplementary Discussion: NW laser threshold
Figures S1-S6

Supplementary Methods

Rate equation analysis in a NW cavity. The carrier density, N, and photon density, P, in the cavity are described by the conventional rate equations in the case of optical pumping[1-3]:

$$\frac{dN}{dt} = \eta_i \frac{L_{in}}{\hbar\omega_p N_w V_1} - \left(AN + BN^2 + CN^3\right) - N_w \Gamma_1 g(N) P$$

$$\frac{dP}{dt} = N_w \Gamma_1 g(N) P - \frac{P}{\tau_p} + \beta BN^2$$

where ω_p is the frequency of a pumping laser, A is the surface nonradiative recombination coefficient, B is the radiative recombination coefficient, C is the Auger nonradiative recombination coefficient, Γ_1 is the single-well confinement factor, V_1 is the single-well volume, and β is spontaneous emission factor. The photon lifetime, τ_p, is represented by $\tau_p = \lambda Q / 2\pi c$, where λ is the wavelength of the output laser, and Q is the quality factor of a resonant mode. The logarithmic gain $g(N) = g_0 (c/n_{eff}) \ln(N/N_{tr})$ was assumed, where g_0 is gain coefficient, N_{tr} is the transparency carrier density, and n_{eff} is the effective refractive index. The absorbed ratio in quantum wells, η_i, can be analytically computed using absorption coefficient, $\alpha \sim 170000$ cm^{-1}, at 266 nm[4,5]. The estimation yielded $\eta_i \sim 0.7$. Then, output power, $L_{out} = \hbar\omega P N_w V_1 / \tau_p$, is plotted as a function of the pump power, L_{in}. To compare the theoretical curves with the experimental data, the pump power was divided by the pumping area and converted to pump power density.

The following material parameters[3, 6-8] for InGaN MQWs are used in the above equations:

$g_0 \sim 2000$ cm^{-1}
$N_{tr} \sim 1.6\text{x}10^{19}$ cm^{-3}
$A \sim 1\text{x}10^{8}$ s^{-1}
$B \sim 3.6\text{x}10^{-11}$ cm^3/s
$C \sim 1\text{x}10^{-32}$ cm^6/s

The remaining optical parameters, including Q and Γ, were computed by three-dimensional FDTD simulation for both 13 and 26MQW NW structures. Solving the above equations using these parameters yielded the curves plotted in Fig. 4c; the same approach and parameters were used to fit the data of inset Fig. 3c with $\beta = 0.03$.

References

1. Baba, T. Photonic crystals and microdisk cavities based on GaInAsP-InP system. *IEEE J. Select. Topics Quantum Electron.* **3**, 808 (1997).
2. Park, H. G. *et al.* Characteristics of modified single-defect two-dimensional photonic crystal lasers *IEEE J. Quantum Electron*. **38**, 1353 (2002).
3. Coldren, L. A. & Corzine, S. W. *Diode lasers and photonic integrated circuits* (Wiley, New York, 1995).
4. Selim Unlu, M. & Strite, S. Resonant cavity enhanced photonic devices *J. Appl. Phys.* **78**, 607 (1995).
5. Muth, J. F. *et al.* Absorption coefficient, energy gap, exciton binding energy, and recombination lifetime of GaN obtained from transmission measurements. *Appl. Phys. Lett.* **71**, 2572 (1997).

6. Smolyakov, G. A., Eliseev, P. G. & Osinski, M. Effects of resonant mode coupling on optical Characteristics of InGaN-GaN-AlGaN lasers. *IEEE J. Quantum Electron*. **41**, 517 (2005).
7. Arif, R. A., Zhao, H. & Tansu, N. Type-II InGaN-GaNAs quantum wells for lasers applications. *Appl. Phys. Lett.* **92,** 011104 (2008).
8. Osinski, M. *et al.* Design of InGaN–GaN–AlGaN vertical-cavity surface-emitting lasers using electrical–thermal–optical simulation. *IEEE J. Sel. Topics in Quantum. Electron.* **7,** 270 (2001).

Supplementary Discussion: NW laser threshold

The laser thresholds of InGaN MQW NWs are higher than optimized GaN NWs reported by our group previously (Ref 10 of paper). We believe that this difference in threshold can be explained in large part by the smaller confinement factor (Γ) in the MQW NW. Γ represents the coupling efficiency between gain medium and resonant modes, and can lead to an exponential change in laser threshold (see main text). To address the importance of Γ, 3D-FDTD simulations were carried out for the two types of structures, where the thickness, refractive index, and emission wavelength of the GaN nanowire are set to be 250 nm, 2.6, and λ = 370 nm, respectively. Supplementary Fig. S5 shows the calculated resonant modes of a bare GaN NW and a GaN/InGaN 26MQW NW. For the bare GaN structure, the whole NW functions as gain medium and yields a large Γ value of 0.92. For the MQW NW structure, the effective gain medium is the shell region and the calculated Γ is 0.24.

To quantify the confinement effects on threshold, we calculated light-in vs. light-out curves (L-L curves) for the bare GaN NW and 26MQW NW lasers. The material parameters of bulk GaN were employed from literature[1]. The L-L curves (Supplementary Fig. S6) yields a threshold of 29.5 kW/cm^2 for bare GaN NW (blue) and 132.8 kW/cm^2 for 26MQW NW lasers (red). The calculated thresholds agree relatively well with the best experimental values of 22 and 400 kW/cm^2, respectively.

These calculations show that the lower values of Γ for the MQW NWs can explain the increased thresholds compared to homogenous GaN NWs. This analysis also suggests that it should be possible to optimize Γ and thereby reduce the threshold in these MQW NW lasers. For example, Γ of a MQW NW structure can be increased by reducing the NW core size to increase the shell/core ratio, or by adding an additional outer GaN/AlGaN cladding layer to modify laser mode profile[2].

In addition, we note that the laser pumping efficiency is determined by the spectral match between the pump wavelength and the absorption band of materials[3]. In our PL studies, it is possible that the mismatch between pumping photons (4.66 eV) and InGaN materials (E_g = 2.51-3.39 eV) could lead to more non-radiative intraband carrier relaxation, which reduces pumping efficiency compared to pure GaN NW structures.

References

1. Mackowiak, P. and Nakwaskiy, W. Detailed threshold analysis of UV-emitting nitride vertical-cavity surface-emitting lasers, *J. Phys. D.* **31**, 2479-2484 (1998).
2. Crisinel, D., Dupertuis, M. -A, and Kapon, E. Vectorial electromagnetic modes in V-shaped dielectric waveguides with application to quantum wire devices, *Optical and Quantum Electronics* **31**, 797 (1999).
3. Koechner, W. *Solid-State Laser Engineering* (Springer, 1999)

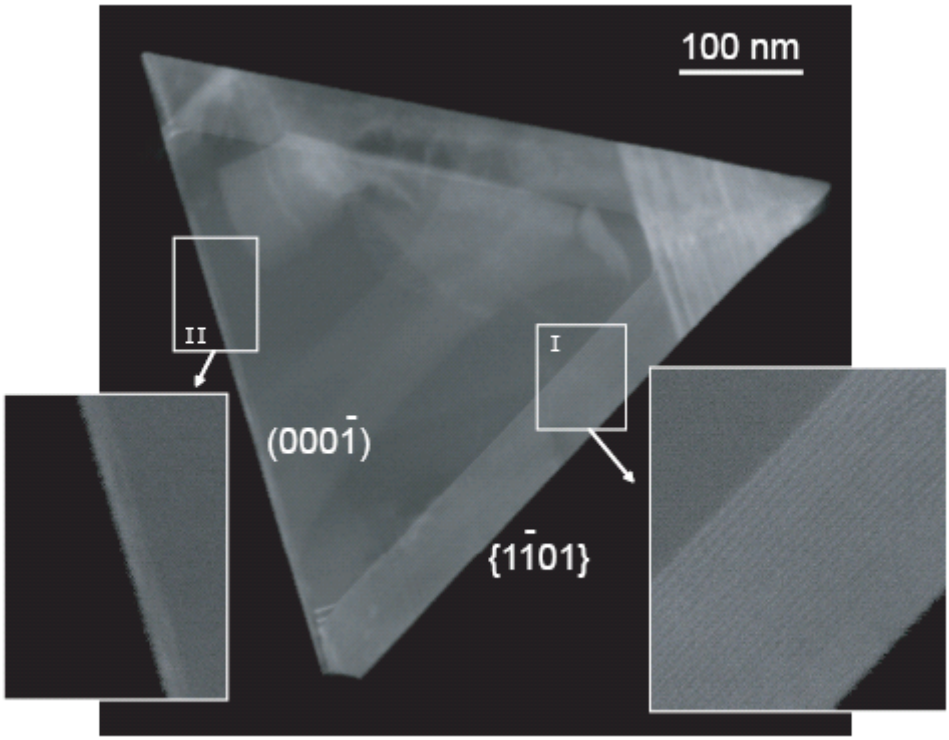

Supplementary Figure S1. Dark-field cross-sectional STEM image of a 26MQW NW structure showing non-uniform shell coating. Scale bar is 100 nm. The image was recorded along the [11-20] zone axis. The white rectangular regions marked as region I and II, showed the magnified part of MQW shell on {1-101} and (000-1) facets, respectively. The main image is the same as in Fig. 1d, and inset from region I is the same as shown in Fig. 1h.

The dark-field STEM image shows that the shell thicknesses on the two crystallographically identical {1-101} planes are the same, and are significantly larger than that of the (000-1) plane. In region I, which is representative of the {1-101} planes, the shell thickness was approximately 65 nm and the 26 periods of InGaN QWs could be resolved clearly with distinct contrast. In region II, which is representative of the (000-1) plane, the shell thickness was estimated to be 10 nm based on the core/shell contrast without observable QW contrast variation.

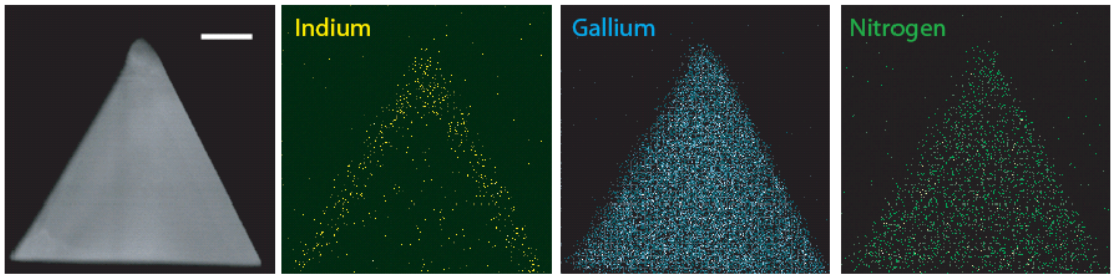

Supplementary Figure S2. Dark-field STEM image of a representative 26MQW NW cross-section and corresponding EDS elemental mapping of In (yellow), Ga (blue) and N (green), respectively. Scale bar is 100 nm. The STEM image and EDS elemental mapping was conducted using a VG HB603 STEM. The distinct profiles confirm that the contrast in the STEM image originate from chemical composition variation, and reveal spatial distribution of these elements. The counts in elemental mapping are directly proportional to the amount and the atomic number of imaged materials. Note the signal-to-noise level is lower for In and N counts, because of their lower composition and atomic number, respectively. The In mapping exhibited a "Λ" shape, consistent with the fact that In is localized in the shells on the {1-101} facets, and that the (000-1) facet has neglectable QW deposition.

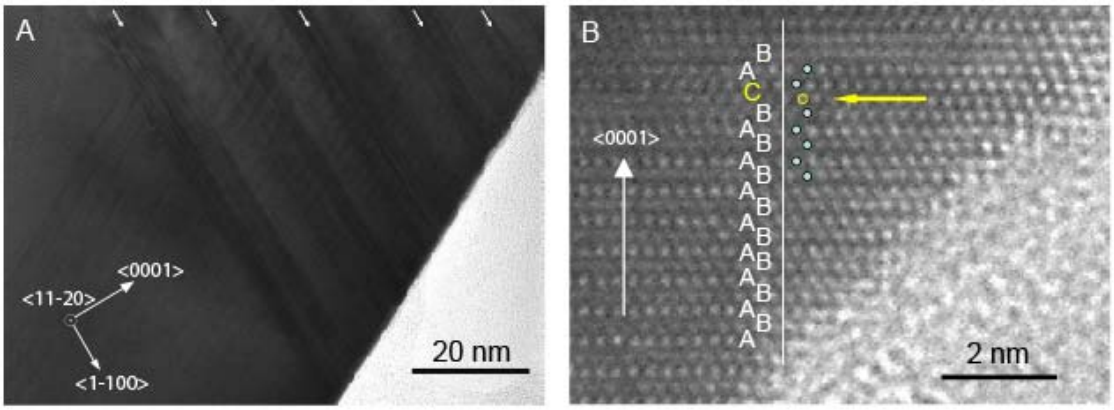

Supplementary Figure S3. Stacking faults in MQW NW structures. (A) Bright-field cross-sectional TEM image of a 26MQW NW corner. The image was recorded along the [11-20] zone axis. The white arrow highlighted the stacking faults observed in the (0001) plane. Scale bar is 20nm. (B) Enlarged TEM image of (A) with atomic resolution. The yellow arrow indicated the position of a stacking fault, in which a change of stacking sequence from AB (wurtzite) to ABC (zinc blende) along <0001> direction was observed. The lattice planes with sequence of AB and C were labeled by blue dots and yellow circle, respectively. The white arrow indicated the <0001> direction in the TEM image, and the white line was guided for eyes. Scale bar is 2nm.

Stacking faults have been reported previously in planar GaN and InGaN materials, and attributed to relaxation of the high residual strain.[1] A recent study on strain relaxation behavior of the InGaN/GaN MQW structure further shows that the strain relaxation is related to the number of QWs.[2] In contrast to conventional planar systems, we do not observe stacking faults on the {1-101} facets, which could have lower strain due to growth on the GaN NW core vs. sapphire substrate, and only observe the stacking faults at intersection between {1-101} facets.

References

1. Choi, H. K., Lee, J. Y., Kim, K. S. & Yang G. M. Phase separation and stacking fault of $In_xGa_{1-x}N$ layers grown on thick GaN and sapphire substrate by metalorganic chemical vapor deposition. *J. Crystal Growth* **220**, 197-203 (2000).
2. Choi, H. K., Lee, J. Y. & Leem, J. Y. Strain relaxation behavior of the InGaN/GaN multiple quantum wells observed by transmission electron microscopy. *Appl. Surf. Science* **221**, 288-292 (2004).

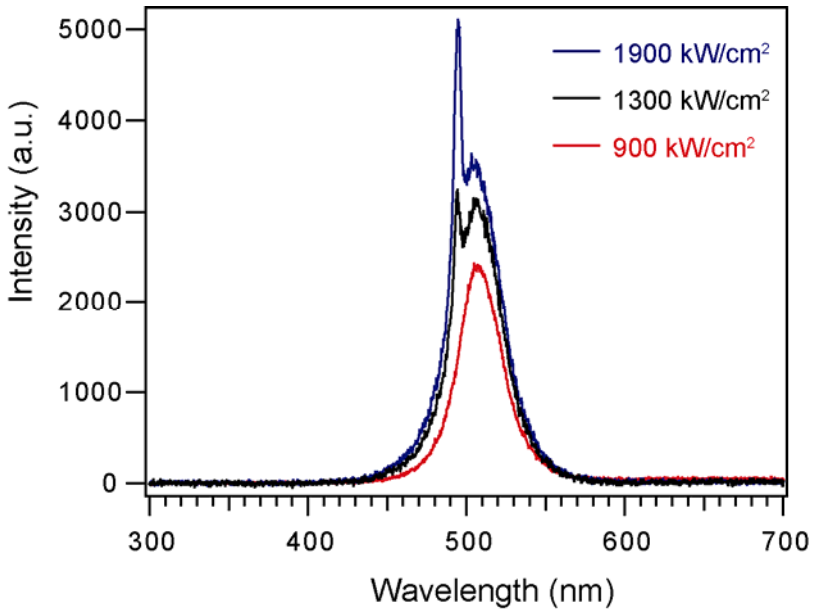

Supplementary Figure S4. Power-dependent PL spectra recorded from a 26MQW NW structure. A sharp peak at 494 nm, which is suggestive of lasing, is observed for power densities above 1300 kW/cm^2. Complete collapse of the spontaneous emission was not observed for range of power densities accessible prior to material damage using 266 nm excitation.

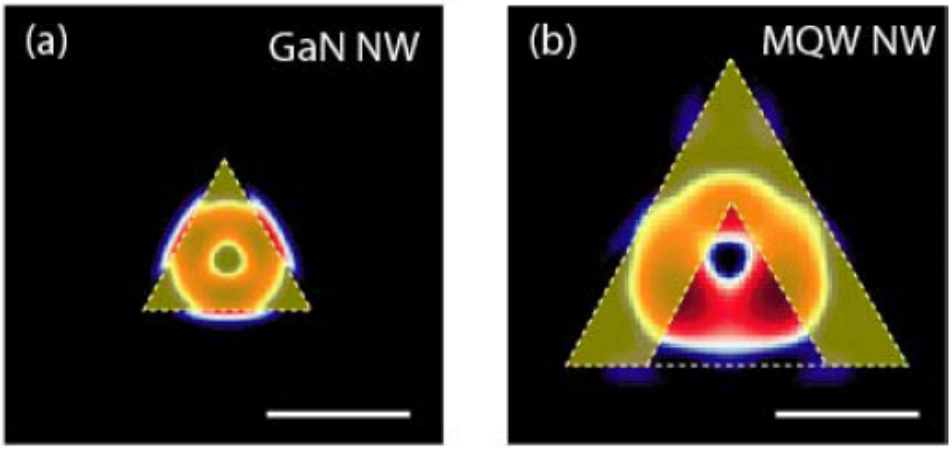

Supplementary Figure S5. Dominant laser modes in a (a) bare GaN NW and (b) GaN/InGaN 26MQW NW structure. Scale bar is 200 nm. The white dashed lines indicated NW/air & core/shell interface, while the yellow area highlighted "effective" gain medium region.

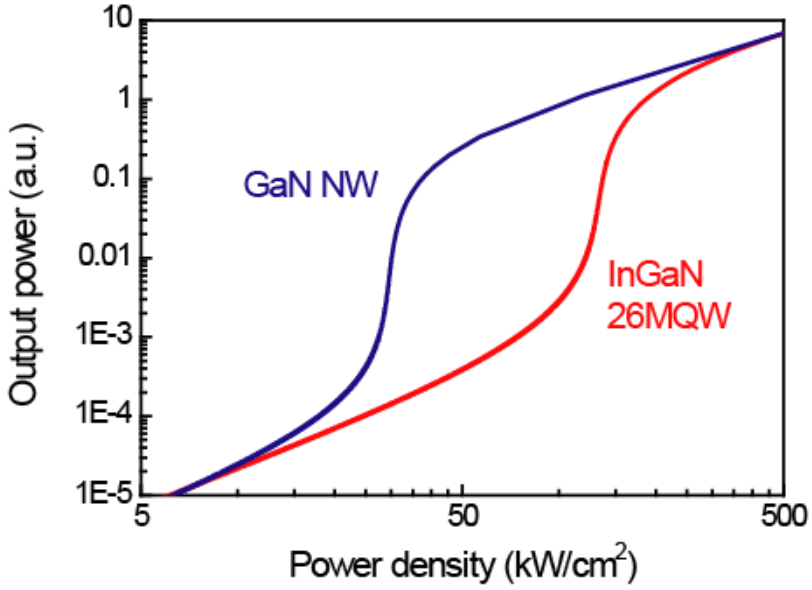

Supplementary Figure S6. Calculated L-L curves for a bare GaN (blue) and GaN/InGaN 26MQW (red) NW lasers.